Eur. J. Biochem. 210, 953–961 (1992)

Time-resolved fluorescence study of human recombinant interferon α_2

Association state of the protein, spatial proximity of the two tryptophan residues

Michel VINCENT[1], Ines M. LI DE LA SIERRA[1, 2], Mário N. BERBERAN-SANTOS[3], Aída DIAZ[2], Maylin DIAZ[2] Gabriel PADRON[2] and Jacques GALLAY[1]

[1] Laboratoire pour l'Utilisation du Rayonnement Electromagnétique, Université Paris Sud, Orsay, France
[2] Centro de Ingeniería Genética y Biotecnología, Habana, Cuba
[3] Centro de Química-Física Molecular, Instituto Superior Técnico, Lisboa, Portugal

(Received September 21, 1992) – EJB 92 1337

Human recombinant interferon α_2 belongs a to family of proteins active against a wide range of viruses. It contains two tryptophan residues located at positions 77 and 141 in the peptide sequence. The fluorescence emission spectrum of these tryptophan residues displays a maximum at 335 nm. The fluorescence intensity decay is described by one broad excited-state-lifetime population centered around a value of 1.7 ns (full width at half maximum, 1.5 ns). These observations suggest that in the native protein, both tryptophan residues emit from similar environments, not directly exposed to the surrounding solvent. The anisotropy decay is essentially biexponential. The correlation-time value characterizing the Brownian rotation of the protein varies linearly with the viscosity/temperature ratio. The calculated hydrodynamic volumes are compatible with the existence of a dimer and a tetramer, at pH 5.5 and 9.4, respectively. Addition of urea at pH 5.5 disrupts the dimer and modifies to some extent the excited-state-lifetime distribution which becomes more heterogeneous. Disulfide-bond reduction also dissociates the dimer and leads to a highly heterogeneous fluorescence-intensity decay with four excited-state-lifetime populations. An opening of the local structure in the Trp region of the protein is likely to occur in these conditions. The fast-anisotropy-decay components can be due to either fast rotation or energy transfer between the indoles. Close proximity of the two Trp residues (less than 1 nm) is suggested from steady-state and time-resolved fluorescence-anisotropy measurements in vitrified medium [95% (by mass) glycerol at −38 °C]. This suggestion is in agreement with the recently published three-dimensional structure of the homologous protein murine interferon β [Senda, T., Shimazu, T., Matsuda, S. Kawano, G., Shimizu, H., Nakamura, K. T. & Mitsui, Y. (1992) *EMBO J. 11*, 3193–3201].

Human (h) recombinant (r) interferon α_2 (IFNα_2) is a 19-kDa protein of 165 amino acids belonging to the cytokine family and is very active in conferring protection against a wide range of viruses [1, 2]. This is therefore an extremely important protein in pathological agression. Unlike that of INFγ [3], its three-dimensional structure, as well as important physicochemical properties, remain unknown, despite attempts to obtain crystals of sufficient quality for X-ray analysis [4]. Several models of protein folding have been proposed [5–9] on the basis of sequence similarity with interleukin 2 [10], and on the relative percentage of α-helical structure deduced from the CD spectrum [11]. These α-helices are assumed to fold to preserve an hydrophobic core [6, 7, 9]. The recently published crystalline structure of the closely related protein murine (m) IFNβ [12, 13] provides some support for these models. One of the best-characterized structural feature of the IFNα family of proteins [12], but which is absent in IFNβ, is the disulfide bond occurring between Cys29 and Cys139. A second disulfide bridge is also present between Cys1 and Cys98, but does not seem to have any biological significance for the physiological role of the molecule [14].

One attractive peculiarity of the IFNα_2 molecule is that it contains two tryptophan residues at positions 77 and 141, respectively, in the N- and C-terminal domains of the protein [15]. Trp141 has been shown to be a 'superconserved' position [2] and is probably an important residue for antiviral activity [16]. Steady-state and time-resolved fluorescence techniques were used to characterize the environment and aggregation state of the protein. Two major conclusions about the structure of hIFNα_2 can be derived from these studies. First, both Trp residues are probably situated in close proximity in the protein three-dimensional structure, not in direct contact with the solvent, in agreement with the recently published three-dimensional structure of the homologous protein mIFNβ [12, 13]. Second, the protein undergoes a pH-dependent self-association process.

MATERIALS AND METHODS

Protein preparation

The hr(IFNγ) and hrIFNα_2 used in this work were obtained by the DNA technique [17, 18], purified then correctly folded (Diaz, A. et al., unpublished results). The re-

Correspondence to M. Vincent, Laboratoire pour l'Utilisation du Rayonnement Electromagnétique, Bâtiment 209D, Université Paris Sud, F-91405 Orsay-Cedex, France

Abbreviations. mem, maximum entropy method; AcTrpNH$_2$, *N*-acetyltryptophanamide; h, human; r, recombinant; IFN, interferon.

sulting proteins are identical to the natural human ones. hrIFNα_2 contains the two disulfide bonds correctly positioned, as verified by MS [19]. Samples were dissolved in 0.1 M ammonium acetate, pH 5.5 or 0.05 M glycine/NaOH, pH 9.4.

Carboxymethylation of the protein was performed according to a modification of the published procedure [20]. Briefly, the protein (1.6 mg/ml) was dissolved in 0.6 M Tris/HCl, pH 8.6, and 6.4 M urea, bubbled with nitrogen. Dithiothreitol (8.6 mM) was added and the mixture was left for 20 min at 40 °C. Excess iodoacetamide (17.8 mM) was added to the protein solution and the reaction proceeded for 40 min in the dark. Excess reactant was eliminated by gel filtration on a Sephadex G-25 column equilibrated with 50 mM sodium acetate, pH 5.5.

Absorbance and fluorescence-intensity measurements

Steady-state fluorescence-emission spectra (excitation band width, 2 nm; emission band width, 4 nm), at room temperature and −38 °C in glycerol, were obtained with a SLM 8000 spectrofluorimeter interfaced to a MacIntosh SE microcomputer. The steady-state anisotropy excitation spectra at −38 °C in glycerol were measured with the same instrument in the T-format mode with a band width of 1 nm at the excitation wavelength using Melles-Griot interference filters (maximum transmission of 30% at λ = 334 nm, 10 nm band width).

Absorption spectra at room temperature were measured on a Cary 2200 spectrophotometer. Measurements at −38 °C in glycerol were performed on a Varian DS200 spectrophotometer equipped with a cryostat device (Oxford). Overlap integral between absorption and emission spectra were calculated from these data.

Fluorescence-intensity and anisotropy decays were obtained by the time-correlated single-photon-counting technique from the polarized components $I_{vv}(t)$ and $I_{vh}(t)$ on the experimental set up installed on the SB_1 window of the synchrotron-radiation machine Super-ACO (Anneau de Collision d'Orsay) which has been described elsewhere [21]. The storage ring provides a light pulse with a full width at half maximum of about 500 ps at a frequency of 8.33 MHz for a double-bunch mode. A Hamamatsu microchannel plate R1564U-06 was utilized. Data for $I_{vv}(t)$ and $I_{vh}(t)$ were stored in separate memories of a plug-in multichannel analyzer card CIC-PC8 (Canberra-France) in a DESKPRO 286E microcomputer (Compaq). Time resolution was 15 ps/channel or 30 ps/channel with 1 K or 2 K channel memory. The instrument response function was automatically monitored in alternation with the parallel and perpendicular components of the polarized fluorescence decay by measuring the scattering of a dilute glycogen solution at the emission wavelength. Automatic sampling of the data was driven by the microcomputer.

Data analysis

Analysis of the fluorescence-intensity and fluorescence-anisotropy decay data as a sum of exponentials was performed by the maximum entropy method (MEM) [21–26]. These programs use MEMSYS 5 (MEDC Ltd, UK) as a library of subroutines.

The principles of MEM, as applied to time-resolved fluorescence, are briefly outlined below.

With a vertically polarized light, the parallel $I_{vv}(t)$ and perpendicular $I_{vh}(t)$ components of the fluorescence intensity at time t after the start of the excitation are

$$I_{vv}(t) = \frac{1}{3} E_\lambda(t) * \int_0^\infty \int_0^\infty \int_{-0.2}^{0.4} \gamma(\tau,\theta,A)\, e^{-t/\tau} \tag{1}$$
$$(1 + 2A\,e^{-t/\theta}) d\tau\, d\theta\, dA$$

and

$$I_{vh}(t) = \frac{1}{3} E_\lambda(t) * \int_0^\infty \int_0^\infty \int_{-0.2}^{0.4} \gamma(\tau,\theta,A)\, e^{-t/\tau} \tag{2}$$
$$(1 - A\,e^{-t/\theta}) d\tau\, d\theta\, dA,$$

where $E_\lambda(t)$ is the temporal shape of the excitation flash, * denotes a convolution product and $\gamma(\tau, \theta, A)$ represents the number of fluorophores with fluorescence lifetime τ, rotational correlation time θ and initial anisotropy A.

Fluorescence intensity decay

The fluorescence-intensity decay is obtained by summing the parallel and perpendicular components:

$$T(t) = I_{vv}(t) + 2I_{vh}(t) = E_\lambda(t) * \int_0^\infty \alpha(\tau) \exp(-t/\tau) d\tau. \tag{3}$$

$\alpha(\tau)$ is the lifetime distribution given by

$$\alpha(\tau) = \int_0^\infty \int_{-0.2}^{0.4} \gamma(\tau,\theta,A)\, d\theta\, dA. \tag{4}$$

In order to ensure that the recovered distribution agrees with the data, S is maximized:

$$S = \int_0^\infty \left[\alpha(\tau) - m(\tau) - \alpha(\tau) \log \frac{\alpha(\tau)}{m(\tau)} \right] d\tau, \tag{5}$$

where $m(\tau)$ is the starting lifetime distribution flat in log τ space and $\alpha(\tau)$ is the resulting distribution.

S was subjected to the following constraint:

$$\sum_{k=1}^{M} \frac{(T_k^{calc} - T_k^{obs})^2}{\sigma_k^2} \leq M, \tag{6}$$

where T_k^{calc} and T_k^{obs} are k calculated and observed intensities. σ_k^2 is the variance of the point k ($\sigma_k^2 = \sigma_{k,vv}^2 + 4\,\beta_{corr}^2\,\sigma_{k,vh}^2$ [27]. M is the total number of observations and β_{corr} is a factor compensating the difference in transmission by the emission monochromator of the parallel and perpendicular light.

The center τ_j of a single class j of lifetimes over the $\alpha(\tau_i)$ distribution is defined as

$$\tau_j = \sum_i \alpha_i(\tau_i)\, \tau_i / \sum_i \alpha_i(\tau_i), \tag{7}$$

the summation being performed on the significant values of the $\alpha_i(\tau_i)$ for class j. C_j is the relative contribution of lifetime class j, such as $\sum_j C_j = 1$. A lifetime domain spanning 150 values, equally spaced on a logarithmic scale between 0.1 ns and 20.0 ns, was routinely used in the analyses. No *a priori* analytical expressions are applied on the shape of the lifetime distribution.

Fluorescence-anisotropy decay in cases of rotational motions

If all the emitting species are assumed to display the same intrinsic anisotropy and rotational dynamics, Eqns (1) and (2) can be rewritten as [26]

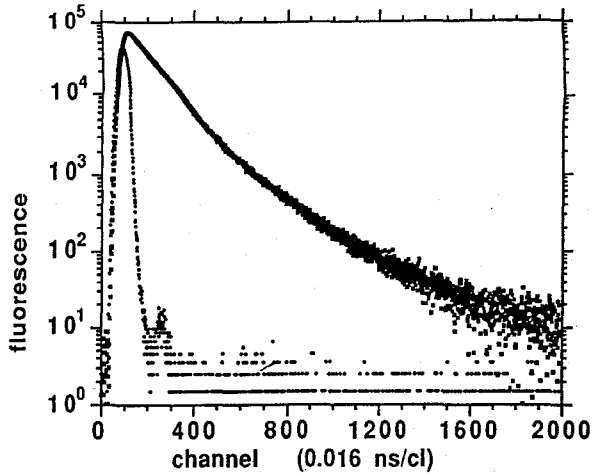

Fig. 1. Fluorescence intensity decay of hr IFNα_2 in 0.1 M acetate, pH 5.5. Excitation wavelength, 300 nm (band width, 5 nm); emission wavelength, 335 nm (band width, 10 nm). cl, channel.

$$I_{vv}(t) = \frac{1}{3} E_\lambda(t) * \int_0^\infty \alpha(\tau) e^{-t/\tau} d\tau [1 + 2 \int_0^\infty \beta(\theta) e^{-t/\theta} d\theta] \quad (8)$$

and

$$I_{vh}(t) = \frac{1}{3} E_\lambda(t) * \int_0^\infty \alpha(\tau) e^{-t/\tau} d\tau [1 - \int_0^\infty \beta(\theta) e^{-t/\theta} d\theta], \quad (9)$$

with

$$A_0 = \int_0^\infty \beta(\theta) d\theta, \quad (10)$$

where $\beta(\theta)$ is the rotational-correlation-time distribution and the other symbols have the same significance as in Eqn (1). The $\alpha(\tau)$ profile is given from a first analysis of $T(t)$ by MEM and is held constant in a subsequent and global analysis of $I_{vv}(t)$ and $I_{vh}(t)$ which provides the distribution $\beta(\theta)$ of correlation times. 100 rotational-correlation-time values, equally spaced in logarithmic scale were used for analysis of $\beta(\theta)$. An infinite time-correlation component can be optionally used in the analysis.

The barycenters of the correlation-time distribution are calculated as

$$\theta_j = \frac{\sum_i \beta_i(\theta_i)\theta_i}{\sum_i \beta_i(\theta_i)}. \quad (11)$$

β_i is the contribution of the rotational correlation time θ_i to class j.

The overall correlation of the rotating particle as a whole can be described simply in an equivalent sphere approximation model as [28]

$$\theta_m = V_h \eta / kT \quad (12)$$

where V_h is the hydrated volume of the particle, η the solvent viscosity and T the absolute temperature. From the correlation-time value, the hydrated volume and the Stokes-radius values can be calculated.

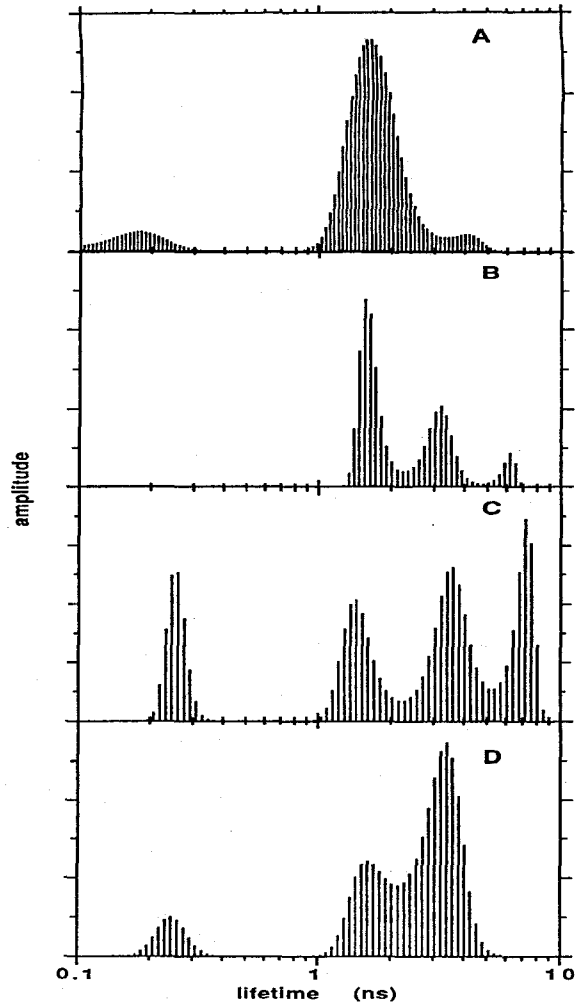

Fig. 2. Excited-state-lifetime profile at 20°C of hrIFNα_2 (17 μM) by MEM. (A) 0.1 M acetate, pH 5.5 (decay parameters: τ_1 = 0.16 ns; τ_2 = 1.64 ns; τ_3 = 3.83 ns; c_1 = 0.10; c_2 = 0.86; c_3 = 0.04; χ-square = 0.997). (B) 7.7 M urea (τ_1 = 1.64 ns; τ_2 = 3.14 ns; τ_3 = 6.05 ns; c_1 = 0.58; c_2 = 0.35; c_3 = 0.07; χ-square = 1.144). (C) Reduced form (τ_1 = 0.26 ns; τ_2 = 1.49 ns; τ_3 = 3.59; τ_4 = 7.01 ns; c_1 = 0.18; c_2 = 0.23; c_3 = 0.35; c_4 = 0.24; χ-square = 0.995). (D) 80% (by vol.) glycerol (τ_1 = 0.25 ns; τ_2 = 1.66 ns; τ_3 = 3.26 ns; c_1 = 0.08; c_2 = 0.28; c_3 = 0.64; χ-square = 1.210). Excitation wavelength: 300 nm (band width, 5 nm) for A, B; 295 nm (band width 5 nm) for C, D. Emission wavelength, 335 nm (band width, 10 nm) for all conditions.

Fluorescence-anisotropy decay in case of energy homotransfer

The rate constant in the case of Förster-type energy transfer (dipole/dipole interaction) [29] contains an orientation factor κ^2 which is often taken as the ensemble average value, 2/3, of the isotropic distribution in the dynamic limit. Experimental protocols to obtain informations about the orientational freedom of dyes and the effect on energy-transfer rates, which can then be measured by the fluorescence-intensity decay, have been proposed [30]. However, in the case of energy transfer between like chromophores (homotransfer), information on transfer rates is only contained in the fluorescence-anisotropy decay, which also contains information on the reorientational-motion rates. Therefore, in order to measure separately the energy-transfer rate in the case of like fluorophores, experiments in conditions where rotational mo-

tion appears extremely unlikely (infinite viscosity) [31] are needed. Recently, the exact anisotropy-decay function in the presence of homotransfer was modelled [32]. The calculations were made under the assumption that (a) there is no preferred orientation between the donor and acceptor, (b) the inter-chromophore distance is constant and identical for all pairs, (c) the direction of the transition moments is not affected by rotational motions during the lifetime of the excited state, and (d) electronic energy transfer occurs via Förster-type dipole/dipole interaction. The calculations were performed by weighing up all the possible configurations without any *a priori* assumption about the orientations. Hence, the expression for the anisotropy decay in the case of homotransfer is [32]

$$A(t) = \frac{A_0}{2}\left\{1 + \int_0^{\pi}\int_0^{\pi}[1 - d_T(\theta,\omega)] \times \exp[-2\,w(\theta,\omega)t] \times \frac{1}{4}\sin\theta\,d\theta\sin\omega\,d\omega\right\}, \quad (13)$$

where A_0 is the fundamental anisotropy. $d_T(\theta,\omega)$ is given by

$$d_T(\theta,\omega) = \frac{1}{4}\left[\frac{3(3\cos^2\theta - 1)^2}{3\cos^2\theta + 1} - 1\right](3\cos^2\omega - 1). \quad (14)$$

$w(\theta,\omega)$ is the transfer rate for each donor/acceptor pair, defined by the expression

$$w(\theta,\omega) = \frac{3}{2}\frac{1}{\tau_D}\left(3\cos^2\theta + 1\right)\cos^2\omega\left(\frac{\overline{R_0}}{r}\right)^6, \quad (15)$$

where τ_D is the excited-state lifetime of the donor, $\overline{R_0}$ is the averaged Förster radius calculated with an effective orientational factor of 2/3, θ is the angle between donor transition moment and the direction joining the donor and acceptor and ω is the angle between the electric field of the donor at the acceptor and the acceptor transition moment [32]. The donor/acceptor distance r can then be calculated from the transfer rate averaged over the angles θ and ω.

For transfer-rate-constant distribution, the Eqn (13) can be rewritten as

$$A(t) = \frac{1}{2}\sum_i v_i\left\{1 + \int_0^{\pi}\int_0^{\pi}[1 - d_T(\theta,\omega)] \times \exp[-2\,w_i(\theta,\omega)t] \times \frac{1}{4}\sin\theta\,d\theta\sin\omega\,d\omega\right\}. \quad (16)$$

The expressions for the polarized components of the fluorescence emission are

$$I_{vv}(t) = \frac{1}{3}E_\lambda(t) * T(t)[1 + 2\,A(t)] \quad (17)$$

and

$$I_{vh}(t) = \frac{1}{3}E_\lambda(t) * T(t)[1 - A(t)], \quad (18)$$

where $E_\lambda(t)$ is the instrument-response function, $T(t)$ is the fluorescence-intensity decay, and * notes a convolution product. The fluorescence-intensity decay was first analyzed by MEM with a set of 50 exponential terms. A global analysis of $I_{vv}(t)$ and $I_{vh}(t)$ by MEM provides the distribution of the transfer-rate-constant values. A set of 50 transfer-rate-constant values was used. Numerical integration over all the relative orientations of the donor/acceptor pairs was performed using steps of 3° for $d\theta$ and $d\omega$.

RESULTS

Steady-state and time-resolved fluorescence-intensity measurements

The fluorescence-emission spectrum of the hr IFNα_2 in 0.1 M acetate, pH 5.5, at room temperature, excited at 300 nm in the absorption-spectral region of the tryptophan residues, displays a maximum at 335 nm (spectrum not shown). The fluorescence-quantum-yield value, calculated with respect to the one of *N*-acetyltryptophanamide (AcTrpNH$_2$) [33], is equal to 0.10. Time-resolved measurements were performed at pH 5.5 and 9.4. The fluorescence-intensity decay is clearly not monoexponential (Fig. 1), but is described by MEM by one major broad excited-state-lifetime distribution centered around 1.7 ns at both pH (Fig. 2A and Table 1). The width at half-peak maximum is about 1.5 ns. Two other lifetimes contribute to a minor extent to the decay. The broad excited-state-lifetime distribution remains essentially unchanged at different excitation and emission wavelengths (Table 1). However, the relative proportion of the minor long component increases in the red edge of the emission spectrum from 0.05 to 0.20 (Table 1). The barycenter value of the broad excited-state-lifetime distribution decreases as a function of temperature from 2 ns to 1 ns in the temperature range 0 – 50 °C (data not shown).

The addition of 7.7 M urea to the protein at pH 5.5 results in a significant change in the lifetime-distribution profile (Fig. 2B). The proportion of the major excited-state population decreases from 95% to about 60% with the same barycenter as in the unperturbed protein. The proportion of the minor 3 – 4-ns component increases to 33%. Moreover, an additional long-lived component (barycenter ≈6 ns) emerges.

A more striking effect on the lifetime-distribution profile is observed after reduction of the protein (Fig. 2C). The major excited-state population of the native protein is still found but with a reduced proportion in the alkylated protein (22% instead of 95%). Two lifetime populations with barycenters similar to those in urea (≈3 and ≈6 ns) are present in higher proportions in the reduced form of the protein. Despite the strong effects on the excited-state decay, only a slight 5-nm red shift is observed in the reduced protein with respect to the native one (maximum emission wavelength, 340 nm, spectrum not shown).

Solvent perturbation of the protein was also performed by adding glycerol to the protein solution. In 80% (by mass) glycerol at room temperature, the fluorescence-intensity decay shows a decrease in proportion of the major lifetime population (28%), to the benefit of the 3 – 4-ns component (63%). A minor component (9%) of barycenter 0.24 ns is also detected (Fig. 2D). At a lower temperature, −38 °C, in 95% glycerol, the decay is described by one major excited-state-lifetime class (85%) of barycenter value 4.3 – 4.7 ns (Table 1) and the 1.7-ns component (15%).

Time-resolved fluorescence anisotropy measurements in aqueous solution: association state of the protein

A first examination of the fluorescence-anisotropy decay shows the existence of depolarization processes occurring in very different time scales. Maximum entropy analysis of the

Table 1. Exited-state-decay parameters of hrIFNα_2 in different experimental conditions. Excitation wavelengths are noted in parentheses. Emission wavelength, 335 nm; except * 320 nm and ** 390 nm. The mean lifetime state, $\langle\tau\rangle$, was calculated as $\sum_i c_i \tau_i$.

Experimental conditions	c_1	c_2	c_3	τ_1	τ_1	τ_2	$\langle\tau\rangle$
				ns			
pH 5.5 (295 nm)	–	0.96	0.04	–	1.71	4.11	1.81
pH 5.5 (300 nm)*	0.19	0.77	0.05	0.98	1.78	4.21	1.77
pH 5.5 (300 nm)	0.08	0.84	0.09	0.40	1.72	4.77	1.75
pH 5.5 (300 nm)**	–	0.80	0.20	–	1.57	2.83	1.82
pH 9.4 (300 nm)	0.02	0.95	0.03	0.40	1.50	4.18	1.56
80% glycerol 20°C (295 nm)	0.08	0.28	0.63	0.25	1.66	3.26	2.54
95% glycerol −38°C (295 nm)	–	0.15	0.85	–	1.71	4.48	4.06

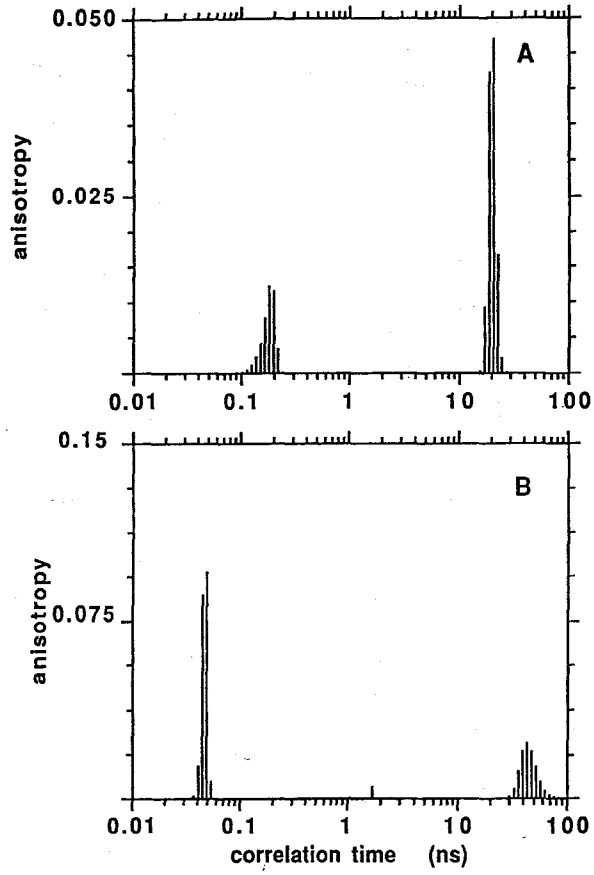

Fig. 3. Correlation-time profile of hrIFNα_2 by MEM. Excitation wavelength, 295 nm. Temperature, 20°C. (A) pH 5.5. Anisotropy-decay parameters: $\theta_1 = 0.18$ ns; $\theta_2 = 20$ ns; $\beta_1 = 0.043$; $\beta_2 = 0.118$; χ-square = 0.999. (B) pH 9.4. Anisotropy-decay parameters: $\theta_1 = 0.05$ ns; $\theta_2 = 45$ ns; $\beta_1 = 0.204$; $\beta_2 = 0.118$; χ-square = 1.019.

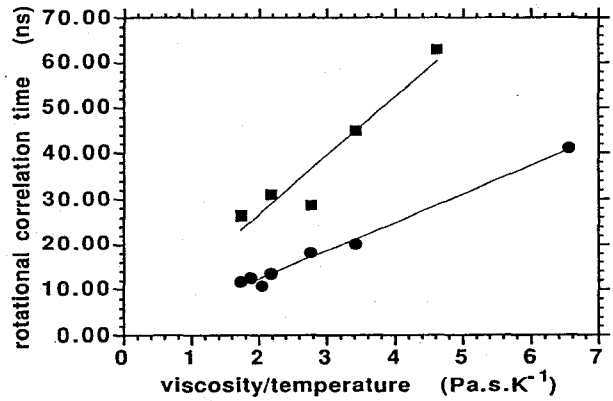

Fig. 4. Perrin representation of the variation of the whole-particle rotational correlation time of hrIFNα^2 as a function of the viscosity/temperature ratio. (●) pH 5.5; (■) pH 9.4. Protein concentration: 17 μM at pH 5.5; 15 μM at pH 9.4.

decay shows that the long correlation time displays a value of 20 ns at pH 5.5 and 20°C (Fig. 3A). At pH 9.4, the long correlation-time value increases up to about 46 ns (Fig. 3B). These correlation-time values are likely to be due to the overall Brownian rotation of the protein. Their variations as a function of the viscosity/temperature ratio are strictly linear, either at pH 5.5 or 9.4 (Fig. 4). The hydrodynamic volumes calculated from each slope give values of 8.6×10^{-26} and 1.78×10^{-25} m^3, at pH 5.5 and 9.4, respectively. The Stokes radii are therefore 2.7 nm and 3.5 nm, respectively. At low temperature and pH 9.4, the correlation time is not measurable owing to the large value of the hydrated volume in these pH conditions and to the limited time window provided by the excited state lifetime (2.15 ns).

Steady-state anisotropy values remain low (0.011 ± 0.002), whatever the protein concentration (0.4−14 μM).

In 7.7 M urea at pH 5.5, the overall correlation time displays an unchanged value of 21 ns as in buffer without urea, and its contribution is the same as in the unperturbed protein. However, the viscosity of the urea solution must be taken into account for proper comparison (≈1.6 mPa · s). Therefore, the value of the rotational-correlation time of the protein, reduced to the water viscosity, must be about 13 ns, a value close to that expected for the monomer. The monomer is also found after reduction of the protein (Table 2).

The presence of fast components (0.05−0.1 ns) of large influence on anisotropy decay are detected whatever the experimental conditions of pH, solvent, temperature or association state of the protein (Table 2). The residual-anisotropy value (the β_3 parameter) after the fast depolarization processes have occurred is not changed to a large extent by temperature, pH or solvent conditions (Table 2).

Steady-state and time-resolved fluorescence anisotropy decay in high-viscosity medium

The fast components observed in the IFNα_2 anisotropy decay (Table 2) may be due either to the fast internal mobility of the indole rings or to the existence of a resonance-energy homotransfer between the two Trp residues [34−36]. This

Table 2. Fluorescence-anisotropy-decay parameters of hrIFNα_2 in different conditions of solvent. Protein concentration, 17 μM. Excitation wavelength was 300 nm, except for the reduced protein, where it was 295 nm.

Sample	Temperature	β_1	β_2	β_3	θ_1	θ_2	θ_3
	°C				ns		
pH 5.5	0	0.093	0.005	0.126	0.05	1.5	41.5
	20	0.043	–	0.118	0.18	–	20.0
	28	0.094	0.004	0.117	0.06	2.0	18.0
	38	0.149	–	0.114	0.04	–	13.5
	45	–	0.011	0.105	–	2.1	12.5
	50	–	–	0.109	–	–	11.4
pH 9.4	10	–	0.005	0.115	–	1.1	63.4
	20	0.204	0.005	0.108	0.05	1.7	46.5
	40	0.042	–	0.096	0.08	–	31.2
	50	0.063	–	0.098	0.18	–	26.5
80% glycerol	20	0.105	0.002	0.100	0.05	0.7	∞
7.7 M urea (pH 5.5)	20	0.032	0.009	0.126	0.08	0.6	21.8 (13.6)[a]
Reduced protein (pH 5.5)	20	–	0.024	0.131	–	0.4	12.5

[a] Value after viscosity correction.

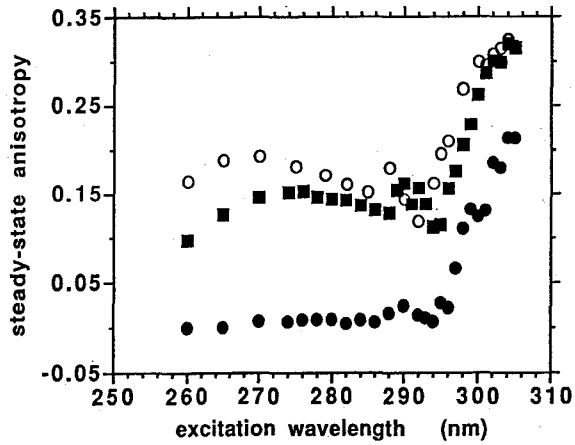

Fig. 5. Steady-state-anisotropy excitation spectra of (○) AcTrpNH$_2$, (●) hrIFNα_2 and (■) hrIFNγ in vitrified medium [80% (by mass) glycerol at −38°C)].

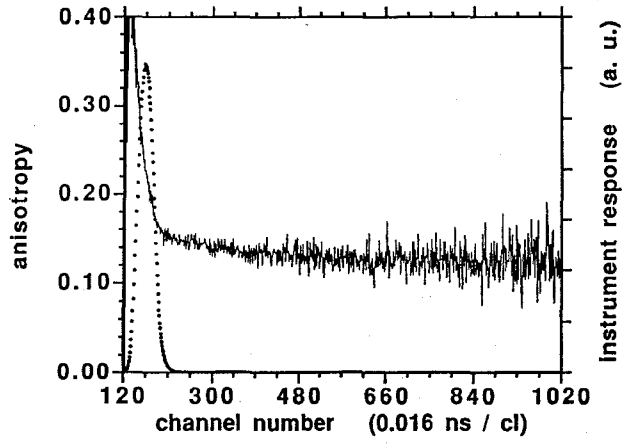

Fig. 6. Experimental anisotropy decay of hrIFNα_2 in 95% (by mass) glycerol at −38°C. Excitation wavelength, 295 nm (band width, 2 nm); emission wavelength, 335 nm (band width, 5 nm). cl, channel.

process can, in fact, only be clearly evidenced by anisotropy measurements in the absence of rotational diffusion. In the presence of rotational motions, the expression of the anisotropy shows that the transfer process is represented by an additional exponential term which is impossible to separate from the exponential decays describing the rotation processes [36]. The experiments were therefore performed in vitrified medium at low temperature.

A first series of measurements were performed under continuous illumination as a function of excitation wavelength. The fundamental anisotropy spectrum of hrIFNα_2 was compared to that of AcTrpNH$_2$. A single tryptophan-containing protein, hrIFNγ, in which the Trp residue is also not completely accessible to the solvent, was also chosen as a test for Trp immobilization in these experimental conditions (Fig. 5). We can observe that the steady-state-anisotropy values of IFNα_2 are much lower than those of AcTrpNH$_2$ at all excitation wavelengths, including the red-edge absorption region. They are also much lower than that of IFNγ, in which energy transfer cannot occur. The anisotropy spectrum of IFNγ is similar to that of AcTrpNH$_2$. At the longest wavelength (>300 nm), both spectra are identical.

Time-resolved-fluorescence-anisotropy-decay measurements in these experimental conditions of viscosity and temperature were also performed. The time dependence of the anisotropy of IFNα_2 in vitrified medium displays a fast initial decrease, then decreases slowly and finally reaches a plateau at 0.1 (Fig. 6). This anisotropy-decay pattern could be in part the result of a residual motion of the indole (but not of the protein itself). However, the analysis of the data by the rotational model (Eqns 8 and 9), shows a continuous distribution of extremely short time constants, the range of which depends on the time window of the calculation. If a window spanning a time constant range of 0.001 − 10 ns is chosen, the resulting time-constant distribution ranges over 1 − 100 ps, with most of the values in the shortest region (Fig. 7A). In a second attempt, a time window spanning a time-constant scale of 0.01 − 10 ns was chosen. The resulting time-constant distribution shows also most of the values in the shortest time-constant range (10 − 60 ps; Fig. 7B). Finally, a third time

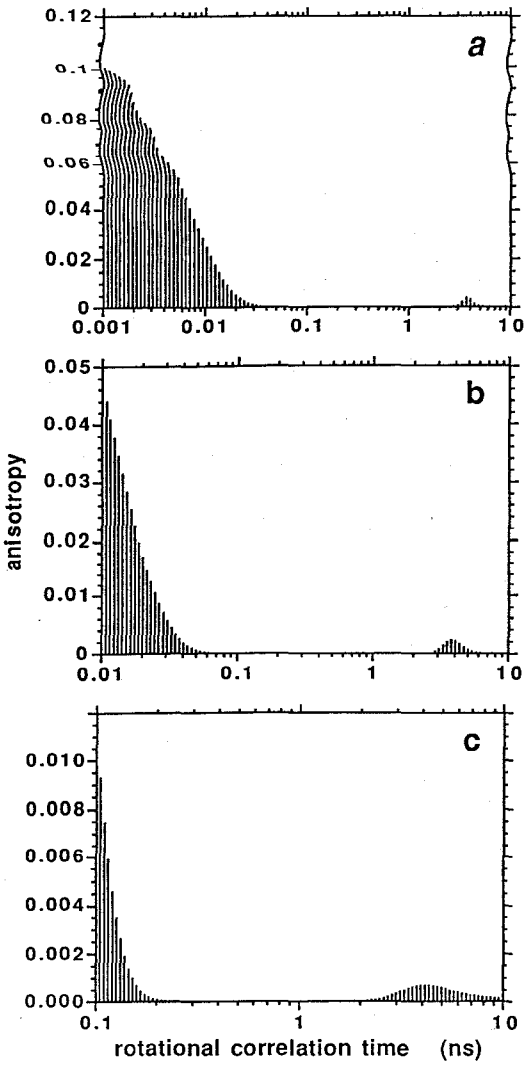

Fig. 7. Rotational-correlation-time-constant profile obtained by MEM analysis of the fluorescence anisotropy decay of hrIFNα_2 in 95% glycerol at −38°C according to the Eqns (8 and 9) described in Materials and Methods with different time windows. A limiting anisotropy value of 0.110, weighing an infinite correlation-time component, was recovered for each analysis (a, b and c).

window provides another different time-constant distribution (Fig. 7C). In the three analyses, a 4-ns time constant, as well as an infinite component corresponding to a plateau value of anisotropy of 0.110, are observed. By contrast, the homotransfer model (Eqn 4) provides a stable transfer-rate profile with a value of 8 ns^{-1} (Fig. 8). The anisotropy at long time is half the anisotropy at time zero, as predicted by the theory [32] and the initial anisotropy value is about 0.2, in reasonable agreement with the usual value observed in the absence of depolarization processes for an excitation wavelength of 295 nm. The weak red-edge effect makes difficult the elimination of the transfer by using a excitation wavelength at the red edge of the absorption spectrum in reasonable conditions of signal/noise ratio [34, 35]. From this transfer-rate value, the Förster critical distance of 1.1 nm, calculated from the spectral overlap integral J and the average excited-state lifetime of 4.4 ns (Table 1), an interchromophore distance of about 0.6 nm, can be calculated.

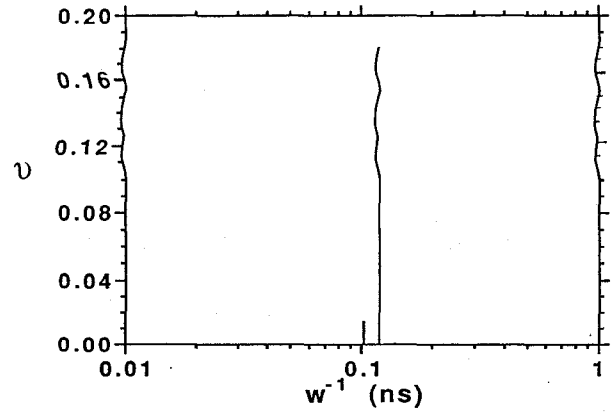

Fig. 8. Energy-transfer-time-constant profile obtained by MEM analysis of the fluorescence-anisotropy decay of hrIFNα_2 in 95% glycerol at −38°C according to the Eqns (16–18) described in Materials and Methods. The calculated parameters are w^{-1} = 0.12 ns; A_0 = 0.195. Excitation wavelength, 295 nm (band width, 2 nm); emission wavelength, 335 nm (band width, 5 nm).

DISCUSSION

The fluorescence emission of IFNα_2 excited above 295 nm is due to the two Trp residues, Trp77 and Trp141. The fluorescence-intensity decay is dominated in all experimental conditions in the native protein by a broad unimodal lifetime distribution which remains identical through the emission spectrum. Minor components are also detected.

One possibility for explaining this comparatively simple lifetime distribution, with regard to some single-Trp-containing proteins [21, 23–25], could be that selective quenching of one of the Trp residues occurs. For instance, the proximity of Trp141 to the disulfide bond formed between Cys29 and Cys139 could result in such an efficient quenching, as is likely to be the case for one pancreatic phospholipase-A_2 mutant, in which Trp94 was stuck between two disulfide bridges [21], or in the case of thioredoxin [24]. However, the average quantum yield and the mean excited-state-lifetime values lead to a mean intrinsic excited-state-lifetime value of 17 ns, quite compatible with those of $AcTrpNH_2$ [37]. Quenching by this above-mentioned disulfide bridge is therefore unlikely. This is consistent with the postulated location of this disulfide bridge in the three-dimensional structure, by comparison with that of the closely related protein IFNβ recently published [12, 13]. These observations suggest that both Trp residues participate in the fluorescence emission.

Therefore, to generate the observed broad lifetime distribution, the decay of each residue should possess close barycenter values indicating similar interactions at the excited state with their environments. The fluorescence-emission spectrum displays a maximum value of 335 nm, suggesting that both indole rings are not directly in contact with the solvent on average. A solvent-shielded localization for both residues is also compatible with the excited-state-lifetime-distribution pattern, since solvent-exposed Trp residues often display large heterogeneities of fluorescence-decay kinetics due to many possibilities of interactions with the solvent molecules or mobile protein groups at the protein surface [21, 23, 38]. More homogeneous fluorescence decays are often observed for solvent-inaccessible Trp residues [39, 40]. This assumed location is in agreement with quenching experiments with iodide or cesium ions [41] and with the structural prediction proposed by Zav'yalov and Denesiuk [9] assuming the folding of several

α-helices shaping a hydrophobic interior. It is also in agreement with the recently published three-dimensional structure of the homologous protein IFNβ, although the coordinates of the amino acid side chains are not available [12, 13]. The Trp77 residue (Trp75 in mIFNβ) is in fact located in the loop joining α-helices B and C. According to the authors, the indole ring of Trp75 is buried, but the two proximal preceding amino acids and the three following ones are exposed. Therefore, it can be sensitive to indirect solvent effects. Trp138, on the other hand, is also buried, but is surrounded by buried residues. The minor contribution of the long-lifetime component, increasing at the red edge of the fluorescence-emission spectrum, could arise from a more solvent-accessible conformation of the first Trp residue. The increased contribution of this lifetime population, after addition of urea or glycerol, reflects the opening of the local protein structure in the Trp region (B–C loop). Reduction of the disulfide bridges induces also a greater accessibility to the solvent of the Trp residues despite the unsensitivity of the secondary structure to these reducing conditions [16].

The fluorescence-anisotropy data provide a set of experimental arguments suggesting that both Trp residues are in fact, as in mIFNβ [12, 13], in close proximity. The comparison of the steady-state anisotropy excitation spectra of $AcTrpNH_2$ and IFNγ suggests that the Trp residues of $IFN\alpha_2$ are probably immobilized in these experimental conditions of high viscosity, although the possibility of weak motions of small amplitude cannot be completely excluded. Examination of the three-dimensional structure of mIFNβ, for which only the Cα backbone is published [12, 13], shows that Trp75 (Trp77 in $IFN\alpha_2$) is located in the B–C loop, a region more mobile than helix E, where Trp138 (Trp141 in $IFN\alpha_2$) is located. However, it is probably sensitive to solvent viscosity, since it is surrounded by exposed residues. The second Trp residue makes close contact with Tyr120 and Tyr121 (Tyr123 and Phe124 in $IFN\alpha_2$). The resulting hydrophobic interactions seem to be important for fixing helix D to the core of the molecule. Therefore, motions of this residue must be limited. Moreover, comparison of the analysis of the anisotropy-decay data by the 'classical' rotational model (Eqns 8 and 9) and by the homotransfer model indicates that the second model is more adapted. The time-constant profiles obtained by the first model are not stable for different time windows used in the analysis. This is in disagreement with the invariance axiom of the coordinate system in the maximum entropy formalism [42]. By contrast, the time-constant profile obtained by the homotransfer model (Eqns 16–18) is stable, in agreement with the above-mentioned principle of MEM formalism. The transfer-rate constant displays a value which allows the calculation of a reasonable interchromophore distance (≈0.6 nm) compatible with the three-dimensional structure of the homologous protein mIFNβ [12, 13]. The distance between the Cα carbon atoms of both Trp residues in mIFNβ is 0.98 nm. At such short distances, the orientation factor is not dominant, but in the absence of the amino acid side-chain atomic coordinates it is not possible to assess this relative orientation in more details.

A further important observation, derived from the anisotropy-decay data, concerns the aggregation state of the protein. In aqueous solution, the overall rotational correlation time of the native protein and its temperature dependence is compatible at pH 5.5 with the existence of a dimer, and at pH 9.4 with that of a tetramer, assuming in both cases a 50% (by mass) hydration ratio. The expected rotational correlation time for such a hydrated monomer should be 10 ns instead of the measured values of 20 ns and 46 ns. The dimer at pH 5.5 is not readily dissociated by dilution in the submicromolar range, as shown by steady-state-anisotropy measurements. By contrast, urea addition and reduction of the protein dissociate the dimer, as shown by the decrease in the rotational correlation time by one half. The dissociation of the dimer does not modify the fast-decaying component of the anisotropy decay and therefore probably not the Trp-Trp energy transfer. Therefore, the possibility of an intermolecular-transfer process involving Trp residues in each monomer of the dimer is unlikely.

In conclusion, these spectroscopic studies provide relevant experimental data on both the local protein structure in the Trp environment and the aggregation state of the $hrIFN\alpha_2$ molecule. The energy-transfer data, as well as the lifetime data, are consistent with the respective location of Trp residues in the three-dimensional structure of the homologous protein IFNβ [12, 13].

The authors wish to thank the CNRS (France)-CECE (Cuba) exchange program for partially supporting in this work. The technical staff of LURE is acknowledged for running the synchrotron machine during the beam sessions. Drs Favaudon and Tétreau (Institut Curie, Orsay) are gratefully acknowledged for the use of the Oxford cryostat and the Varian DS200 spectrophotometer. This work was partially granted by INSERM (CRE 910915).

REFERENCES

1. Isaacs, A. & Lindenmann, J. (1957) *Proc. R. Soc. Lond. Ser. B 147*, 258–267.
2. De Maeyer, E. & de Maeyer-Grignard, J. (1989) *Interferons and other related cytokinines*, John Wiley and Sons, New York.
3. Ealick, S. E., Cook, W. J., Vijay-Kumar, S., Carson, M., Nagabushan, T. L., Trotta, P. P. & Bugg, C. E. (1991) *Science 252*, 698–702.
4. Miller, D. L., Kung, H. & Pestka, S. (1982) *Science 215*, 689–690.
5. Lancer, J. A. & Petska, S. (1965) *Pharmacol. & Ther. 27*, 371–401.
6. Sternberg, M. J. E. & Cohen, F. E. (1982) *Int. J. Biol. Macromol. 4*, 137–144.
7. Zav'yalov, V. P. & Denesyuk, A. I. (1984) *Proc. Natl Acad. Sci. USSR 275*, 242–246.
8. Ptisyn, O. B., Finkelstein, A. V. & Murzin, A. G. (1985) *FEBS Lett. 186*, 143–148.
9. Zav'yalov, V. P., Denesyuk, A. I. & Zav'yalova, G. A. (1989) *Immunol. Lett. 22*, 173–182.
10. Brandhuber, B. J., Boone, T., Kenney, W. C. & McKay, D. B. (1987) *Science 238*, 1707–1709.
11. Bewley, T. A., Levine, H. L. & Wetzel, R. (1982) *Int. J. Pept. Protein Res. 20*, 93–96.
12. Senda, T., Matsuda, S., Kurihara, H., Nakamura, K. T., Kawano, G., Shimizu, H., Mizuno, H. & Mitsui, Y. (1990) *Proc. Jpn Acad. Ser. B, Phys. Biol. Sci. 33*, 77–80.
13. Senda, T., Shimazu, T., Matsuda, S. Kawano, G., Shimizu, H., Nakamura, K. T. & Mitsui, Y. (1992) *EMBO J. 11*, 3193–3201.
14. Wetzel, R., Johnston, P. D. & Czarniecki, C. W. (1983) in *Biology of the interferon system* (de Maeyer, E. & Schellenkens, H., eds) pp. 101–120, Elsevier, Amsterdam.
15. Edge, M. D., Camble, R., Moore, V. E., Hockney, R. C., Carr, F. J. & Fitton, J. E. (1986) *Interferon 7*, 2–46.
16. Wetzel, R., Levine, H. L., Estell, D. A., Shire, S., Finer-Moore, J., Stround, R. M. & Bewley, T. A. (1982) *UCLA Symp 25*, pp. 365–376.
17. Quiñones, Y., Agraz, A., Silva, A., Padrón, G., Mella, C., Diaz, R., Quintana, M., Gonzáles, M., Besada, V., Duarte, C., Sierra, G., Fernández, J., Ubieta, R., Morales, J., Castellanos, L.,

Morera, V., Furrazola, G., Monero, M., Santos, A., Diaz, A. & Herrera, L. (1989) *Highlights Mod. Biochem. 2*, 1237–1246.
18. Perez, L., Vega, J., Chuay, C., Menendez, A., Ubieta, R., Montero, M., Padrón, G., Silva, A., Santizo, C., Besada, V. & Herrera, L. (1990) *Appl. Microbiol. Biotechnol. 33*, 429–434.
19. Padrón, G., Besada, V., Agraz, A., Quiñones, Y. & Herrera, L. (1989) *Anal. Chim. Acta 223*, 361–369.
20. Crestfield, A. M., Stanford, M. & William, H. S. (1962) *J. Biol. Chem. 238*, 622–627.
21. Kuipers, O. P., Vincent, M., Brochon, J. C., Verheij, H. M., de Haas, G. H. & Gallay, J. (1991) *Biochemistry* 30, 8771–8785.
22. Livesey, A. K. & Brochon, J. C. (1987) *Biophys. J. 52*, 693–706.
23. Vincent, M., Brochon, J. C., Merola, F., Jordi, W. & Gallay, J. (1988) *Biochemistry 27*, 8752–8761.
24. Merola, F., Rigler, R., Holmgren, A. & Brochon, J. C. (1989) *Biochemistry 28*, 3383–3398.
25. Gentin, M., Vincent, M., Brochon, J. C., Livesey, A. K. & Gallay, J. (1990) *Biochemistry 29*, 10405–10412.
26. Vincent, M. & Gallay, J. (1991) *Eur. Biophys. J. 20*, 183–191.
27. Wahl, Ph. (1979) *Biophys. Chem. 10*, 91–104.
28. Perrin, F. (1926) *J. de Physique 7*, 390–401.
29. Förster, T. (1948) *Ann. Physik 2*, 55–75.
30. Dale, R. E., Eisinger, J. & Blumberg, W. E. (1979) *Biophys. J. 26*, 161–194.
31. Weber, G. (1960) *Biochem. J. 75*, 345–352.
32. Berberan-Santos, M. N. & Valeur, B. (1991) *J. Chem. Phys. 95*, 8048–8055.
33. Werner, T. C. & Forster, L. S. (1979) *Photochem. Photobiol. 29*, 905–914.
34. Spencer, R. D. & Weber, G. (1970) *J. Chem. Phys. 52*, 1654–1663.
35. Weber, G. & Shinitzky, M. (1970) *Proc. Natl. Acad. Sci. USA 65*, 823–830.
36. Bastiaens, P. H., Bonants, P. J. M., Müller, F. & Visser, A. J. W. G. (1989) *Biochemistry* 28, 8416–8425.
37. Privat, J. P., Wahl, Ph. & Auchet, J. C. (1979) *Biophys. Chem. 9*, 223–233.
38. Petrich, J. W., Longworth, J. W. & Fleming, G. R. (1987) *Biochemistry 26*, 2711–2722.
39. James, D. R., Demmer, D. R., Steer, R. P. & Verall, D. E. (1985) *Biochemistry 24*, 5517–5526.
40. Chen, L. X.-Q., Longworth, J. W. & Fleming, G. R. (1987) *Biophys. J. 51*, 865–873.
41. Borukhov, S. I. & Strongin, A. Ya. (1990) *Biochem. Biophys. Res. Commun. 169*, 282–288.
42. Livesey, A. K. & Skilling, J. (1985) *Acta Crystallogr. Sect. B Struct. Crystallogr. Cryst. Chem. A41*, 113–122.